iScience

Article

Oxidative stress induced protein aggregation via GGCT produced pyroglutamic acid in drug resistant glioblastoma

Graphical abstract

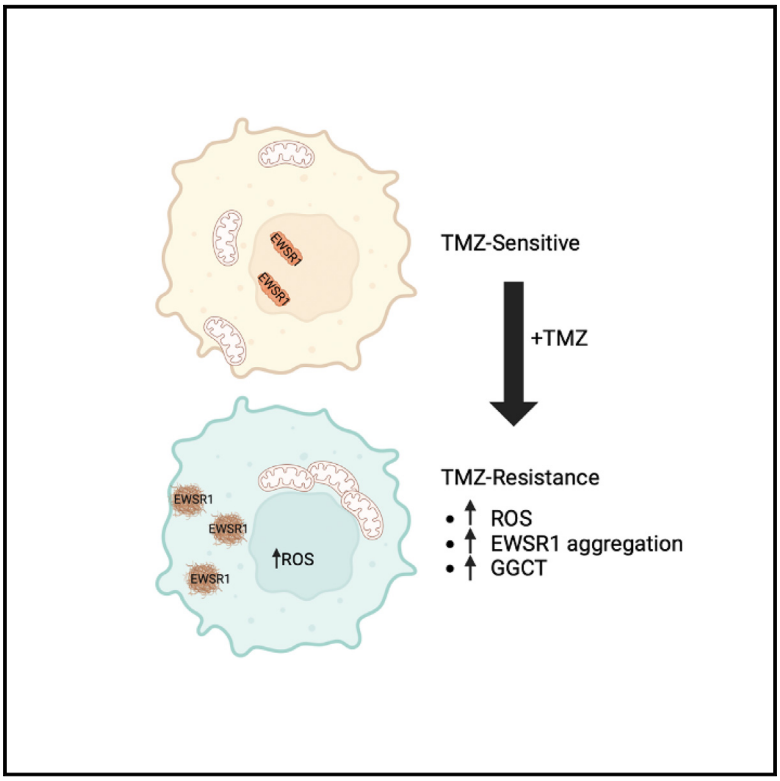

Highlights

- Drug resistance in GBM affects the overall metabolic state, increasing oxidative stress
- Increasing oxidative stress induces the aggregation of EWSR1—in an endogenous model
- GGCT affects EWSR1 aggregation via pyroglutamic acid in both GBM and AD patients

Authors

Deanna Tiek, Xiao Song, Xiaozhou Yu, ..., Jason Miska, Bo Hu, Shi-Yuan Cheng

Correspondence

deanna.tiek@northwestern.edu (D.T.), shiyuan.cheng@northwestern.edu (S.-Y.C.)

In brief

Biological sciences; Neuroscience; Molecular neuroscience; Cancer

Tiek et al., 2025, iScience *28*, 111769
February 21, 2025
https://doi.org/10.1016/j.isci.2025.111769

CellPress

iScience

CellPress
OPEN ACCESS

Article

Oxidative stress induced protein aggregation via GGCT produced pyroglutamic acid in drug resistant glioblastoma

Deanna Tiek,[1,6,*] Xiao Song,[1] Xiaozhou Yu,[1] Runxin Wu,[1] Rebeca Iglesia,[1] Alicia Catezone,[2] Katy McCortney,[2] Jordain Walshon,[2] Craig Horbinski,[2] Pouya Jamshidi,[3] Rudolph Castellani,[3] Robert Vassar,[4] Jason Miska,[5] Bo Hu,[1] and Shi-Yuan Cheng[1,*]

[1]The Ken & Ruth Davee Department of Neurology, The Lou and Jean Malnati Brain Tumor Institute, The Robert H. Lurie Comprehensive Cancer Center, Simpson Querrey Institute for Epigenetics, Northwestern University Feinberg School of Medicine, Chicago, IL 60611, USA
[2]Departments of Pathology and Neurological Surgery, The Lou and Jean Malnati Brain Tumor Institute, The Robert H. Lurie Comprehensive Cancer Center, Northwestern University Feinberg School of Medicine, Chicago, IL 60611, USA
[3]Department of Pathology, Northwestern University Feinberg School of Medicine, The Mesulam Center for Cognitive Neurology and Alzheimer's Disease, Chicago, IL 60611, USA
[4]The Ken & Ruth Davee Department of Neurology, Northwestern University Feinberg School of Medicine, The Mesulam Center for Cognitive Neurology and Alzheimer's Disease, Chicago, IL 60611, USA
[5]Department of Neurosurgery, The Lou and Jean Malnati Brain Tumor Institute, The Robert H. Lurie Comprehensive Cancer Center, Northwestern University Feinberg School of Medicine, Chicago, IL 60611, USA
[6]Lead contact
*Correspondence: deanna.tiek@northwestern.edu (D.T.), shiyuan.cheng@northwestern.edu (S.-Y.C.)
https://doi.org/10.1016/j.isci.2025.111769

SUMMARY

Drug resistance is a major barrier to cancer therapies and remains poorly understood. Recently, non-mutational mechanisms of drug resistance have been proposed where a more plastic metabolic response can play a major role. Here, we show that upon drug resistance, glioblastoma (GBM) cells have increased oxidative stress, mitochondria function, and protein aggregation. Gamma (γ)-glutamylcyclotranserase (GGCT), an enzyme in the γ-glutamyl cycle for glutathione production, located on chromosome 7 which is commonly amplified in GBM is also increased upon resistance. We further observe that the byproduct of GGCT—pyroglutamic acid—can bind aggregating proteins and that genetic and pharmacological inhibition of GGCT prevents protein aggregation. Finally, we found increased protein aggregation, GGCT expression, and pyroglutamic acid staining in recurrent GBM patient samples, adjacent non-tumor brain, and Alzheimer's brains. These findings suggest a new pathway for protein aggregation within drug resistant brain cancer that should be further studied in other brain disorders.

INTRODUCTION

Protein aggregation is a hallmark of neurological diseases like Alzheimer's, Huntington's, and amyotrophic lateral sclerosis[1]; however, the role of protein aggregation in brain cancers has been less thoroughly studied.[2] Glioblastoma (GBM) is the most malignant form of brain cancer, with a median overall survival of ∼21 months.[3] The current standard of care therapy is the Stupp protocol which consists of surgery, radiation, and the chemotherapeutic agent temozolomide (TMZ).[4] While initially successful in some patients, TMZ resistance is rapid and uniformly fatal, where a better mechanistic understanding of TMZ-resistant (TMZ-R) disease may lead to better therapeutic targets.[5]

Previous work has suggested a role for both oxidative stress and glutathione (GSH) changes upon drug resistance in cancers.[6,7] One of the major antioxidant pathways within the cell is GSH production.[8] GSH is a tripeptide synthesized from cysteine, glutamate, and glycine where the thiol of cysteine acts as a cofactor for antioxidant enzymes in their detoxification of reactive oxygen species (ROS).[9] This is in contrast to the role of the mitochondria, where complexes I[10] and III[11] are major producers of ROS, which have been shown to increase upon drug resistance in many cancer types.[12] This is further shown with drug resistant cells which show a downregulation of the antioxidant response, and an increase in ROS.[7] The interplay of ROS production via the mitochondria and detoxification via GSH is therefore an important system when studying drug resistant disease.[13]

The brain is especially sensitive to oxidative damage as it consumes about 20% of the total oxygen in the body due to the high energy demand of maintaining neuronal signaling.[14] In neurological diseases, like familial amyotrophic lateral sclerosis (ALS), ∼10–20% of cases have superoxide dismutase 1 (SOD1)[15] mutations that turn this antioxidant enzyme to a pro-oxidant enzyme and increases protein aggregate deposition.[16–18] However,

other metabolic products have also been shown to seed protein aggregates, such as tyrosine (Tyr),[19] phenylalanine (Phe),[20] quinolinic acid,[21] and more recently poly(ADP-ribose) (PAR).[22] This suggests a dual role of metabolism where oxidation and metabolic byproducts can both play a role in protein aggregation, as a hallmark of brain disorders.

Here, we report that GSH metabolism is dysregulated in TMZ-R GBM where the metabolic byproduct, pyroglutamic acid, is increased and able to seed protein aggregates. While previous work in Alzheimer's focuses on glutaminyl cyclase (QC) as the main producer of pyroglutamic acid,[23] we found the GSH enzyme, gamma (γ)-glutamylcyclotranserase (GGCT), to be responsible for producing pyroglutamic acid which can bind protein aggregates in TMZ-R GBM—with a role for both the function and localization of mitochondria. Finally, we found that this GGCT/pyroglutamic acid/protein aggregate axis in TMZ-R patient samples, adjacent non-tumor brain, and Alzheimer's brains where future work can determine new avenues for therapeutic gain in these differentially oxidized tumors with pyroglutamic acid bound aggregates as a potential biomarker for treatment.

RESULTS

Oxidative stress homeostasis is dysregulated in TMZ-resistant GBM

Drug resistance is a major clinical barrier[24] where we sought to evaluate a non-mutational based vulnerability in TMZ-R GBM. As others have shown drug resistant cells to have a dysregulated antioxidant response,[7] we used patient-derived isogenic TMZ-sensitive (TMZ-S; 42WT) and TMZ-R (42R) GBM cell models[25] to test intracellular pH changes and found a decreased pH in TMZ-R models (Figure 1A; a higher pHrodo reading correlates to a lower pH[26]). This intracellular pH change was also noted in the cell media where TMZ-R cells had a decreased extracellular pH (Figure 1B). Next, we performed untargeted metabolomics and found pyrimidine and glutathione metabolism to be among the most significantly altered pathways between TMZ-S and -R cells (Figure 1C). As pyrimidine synthesis has been studied extensively in gliomas,[27–29] we focused on GSH metabolism where GSH is a major antioxidant in the cell used to combat increased ROS.[30] We next quantified intracellular ROS and found increased ROS in TMZ-R models as compared to TMZ-S lines (Figure 1D). Previous work has correlated increased oxidative stress to increased protein aggregation,[31] where we previously showed TMZ-R models have an increase in the aggregation of EWSR1—a member of the Fus, EWSR1, and Taf15 (FET) family.[32] To determine the effect of decreased ROS on protein aggregation, we treated TMZ-R cells with the general antioxidant N-acetyl cysteine (NAC)[33] and found a decrease in protein aggregates (Figure 1E). Furthermore, we observed that antioxidant treatment decreased TMZ-R cell growth but increased TMZ-S growth (Figure 1F). These results suggest that maintained ROS levels are beneficial for TMZ-R lines, with NAC affecting EWSR1 protein aggregation.

Perinuclear mitochondria are prevalent and more active in TMZ-R GBM

As mitochondria are the main producers of ROS,[34] we next measured mitochondrial function using a Seahorse stress test and found an increased oxygen consumption rate (OCR) in TMZ-R lines compared to TMZ-S (Figure 2A, Figure S1A, related to Figure 2). This increase in mitochondrial OCR in TMZ-R cells was accompanied by an increase in the extracellular acidification rate (ECAR) (Figure 2B),[35] which corroborated the decrease in pH noted in Figure 1. To quantify the relative abundance of mitochondria in each cell, we stained cells with MitoTracker[36] to quantify total fluorescence but found no change in mitochondrial abundance (Figure 2C). However, upon staining cells with MitoTracker, we observed an increase in perinuclear mitochondria in TMZ-R lines as compared to TMZ-S (Figure 2D). This was accompanied by an increase in nuclear 8-oxo-deoxyguanine (8-oxoG), an oxidized base which is commonly used as a marker of increased oxidative stress (Figure 2E).[37] Previous work has shown that perinuclear mitochondria can lead to an increase in 8-oxoG and affect protein binding to DNA, but that a short, low-dose nocodazole (noc) treatment can redistribute mitochondria and decrease 8-oxoG accumulation.[38] We therefore tested this possibility with 10 nM Noc treatment of GBM cells for 45 min and found that mitochondria became more cytoplasmic/spread (Figure 2F). Furthermore, nuclear 8-oxoG also decreased with nocodazole treatment and increased with acute TMZ treatment (Figures 2G and 2H). Lastly, we show a decrease in 8-oxoG accumulation with NAC, suggesting a signaling role for 8-oxoG rather than a mutational or DNA repair deficiency (Figure 2I).

GSH intermediate protein, GGCT, is increased in TMZ-R GBM

We next investigated the role of the γ-glutamyl cycle as GSH production inadequate to decrease ROS levels in TMZ-R cells. The γ-glutamyl cycle consists of multiple enzymes that start with a γ-glutamyl-amino acid (AA) that is converted to pyroglutamic acid, then glutamate, next a cysteine is added to create γ-glutamic acid (Glu)-cysteine (Cys), where finally a glycine (Gly) is added to make the tripeptide GSH (Figure 3A).[39,40] In comparing TCGA,[41] CGGA,[42] and Rembrandt[43] datasets, we found the enzyme GGCT to have the highest clinical relevance with an increased expression leading to lower overall survival (OS) in both the primary, but more significantly in recurrent disease—as well as in higher grade gliomas (Figure 3B, Figures S2A–S2D, S2H, and S2I, related to Figure 3). Furthermore, when looking at the location of GGCT within the genome, it is located on chromosome 7,[44] which is frequently gained in IDH wild type (WT) GBM[45]—but not in IDH mutant lower grade gliomas—and adjacent to genes involved with complex III function within the mitochondria—as well as EGFR (Figure 3C). Within our models, we found an increase in GGCT expression at the protein level (Figure 3D). Furthermore, looking at single cell datasets, we found GGCT and the complex III proteins to be more expressed in glioma cells (Figure S2J, related to Figure 3), and within glioma cell states, GGCT was most expressed in the G1.S state (Figure S2K, related to Figure 3). Overexpression of GGCT increased cell growth in both TMZ-S and -R models (Figure 3E), whereas introduction of a catalytically dead mutant (E98A) [44] only affected cell growth in TMZ-R models (Figure 3E). GGCT has been shown to have two roles in the γ-glutamyl cycle. First, it catalyzes the step from a γ-glutamyl-amino acid to pyroglutamic acid. However, it can also hydrolyze γ-Glu-Cys back to pyroglutamic acid

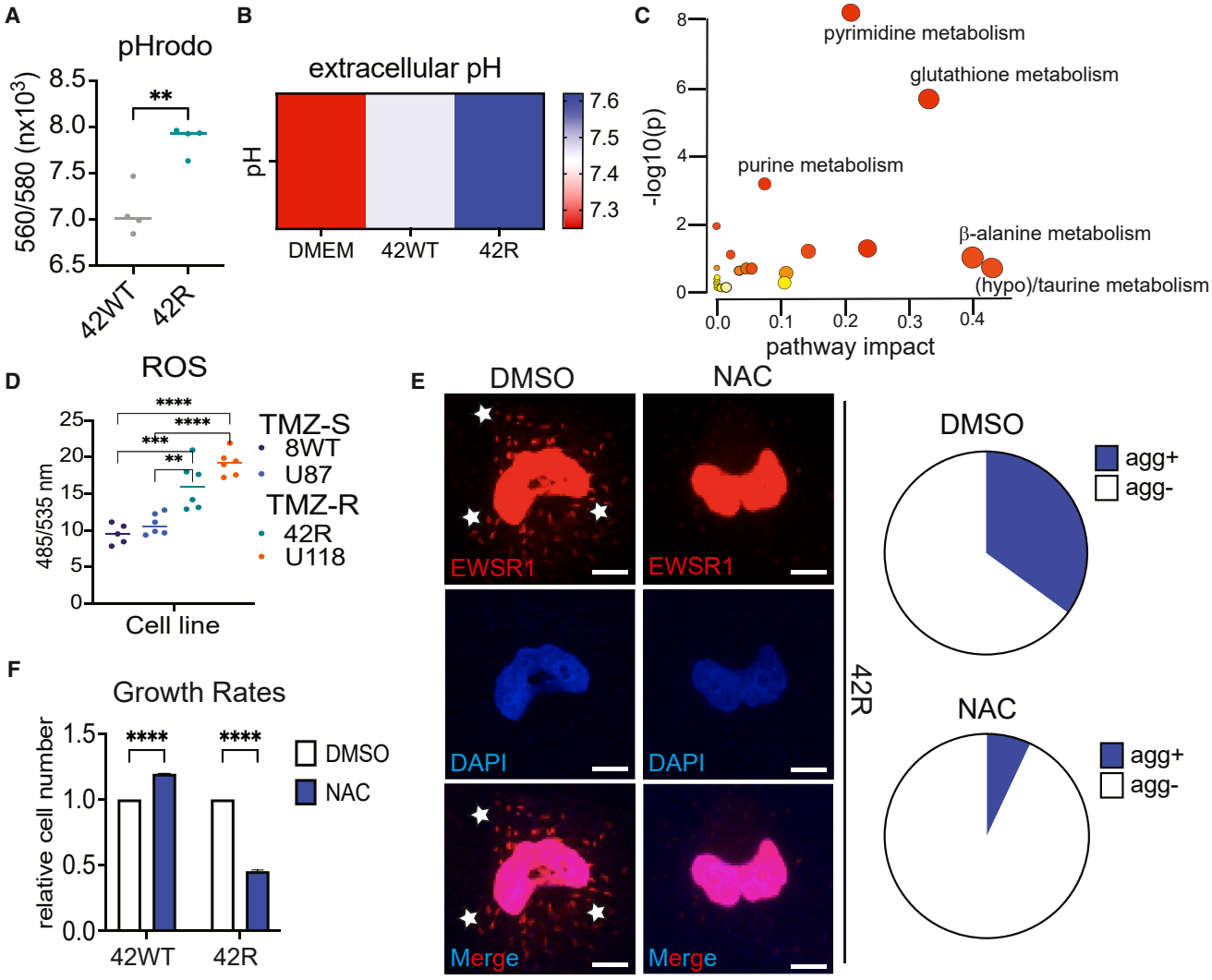

Figure 1. Oxidative stress in TMZ-resistant GBM

(A) pHrodo absorbance reading in denoted cells for inverse pH, t test.

(B) pH reading of cell media in denoted cells post 48 h.

(C) Pathway analysis on Metaboanalyst for metabolomics of denoted cells.

(D) DCFDA absorbance in denoted cells for ROS abundance, one-way ANOVA.

(E) Immunofluorescence (IF) of 42R cells with EWSR1 and nuclear (DAPI) staining = /- DMSO or N-acetyl cysteine (NAC) at 1 mM for 12 h; Pie graphs on the right, quantification of total cell aggregates (aggs) scale bar, 5 μm.

(F) Crystal violet assay of cell growth with 1 mM NAC for 24 h treatment, t test.

All error bars are SD; *$p < 0.05$, **$p < 0.001$, ***$p < 0.0005$, and ****$p < 0.0001$.

and Cys.[46] Re-analyzing our metabolomics data we found an increase of both pyroglutamic acid and γ-Glu-Cys in TMZ-R cells (Figure 3G). As the next step in GSH synthesis after γ-Glu-Cys is the addition of glycine,[39] we reasoned that the γ-Glu-Cys intermediate may be more abundant because of a decrease in glycine. Accordingly, glycine had a trend to decrease in TMZ-R cells (Figure S2E, related to Figure 3), possibly being used for *de novo* GTP synthesis, as has been previously shown in TMZ-R GBM (Figure S2F, related to Figure 3).[46] Additionally, treatment with glycine, GTP and GSHee, a cell permeable version of GSH,[47] all decreased aggregate formation (Figure S2G, related to Figure 3). Furthermore, inhibiting GCase, which synthesizes γ-Glu-Cys, had no effect on TMZ-R growth. However, the GGCT inhibitor, ProGA,[48] decreased cell growth in TMZ-R lines as compared to TMZ-S lines (Figure 3F) suggesting a specific role for pyroglutamic acid/GGCT in TMZ-R GBM.

Pyroglutamic acid binds to EWSR1 protein aggregates

Pyroglutamic acid has previously been shown to co-stain with aggregating proteins, such as amyloid beta in Alzheimer's disease.[49] We therefore wondered if it might play a similar role in TMZ-R GBM as we have previously published the RNA binding

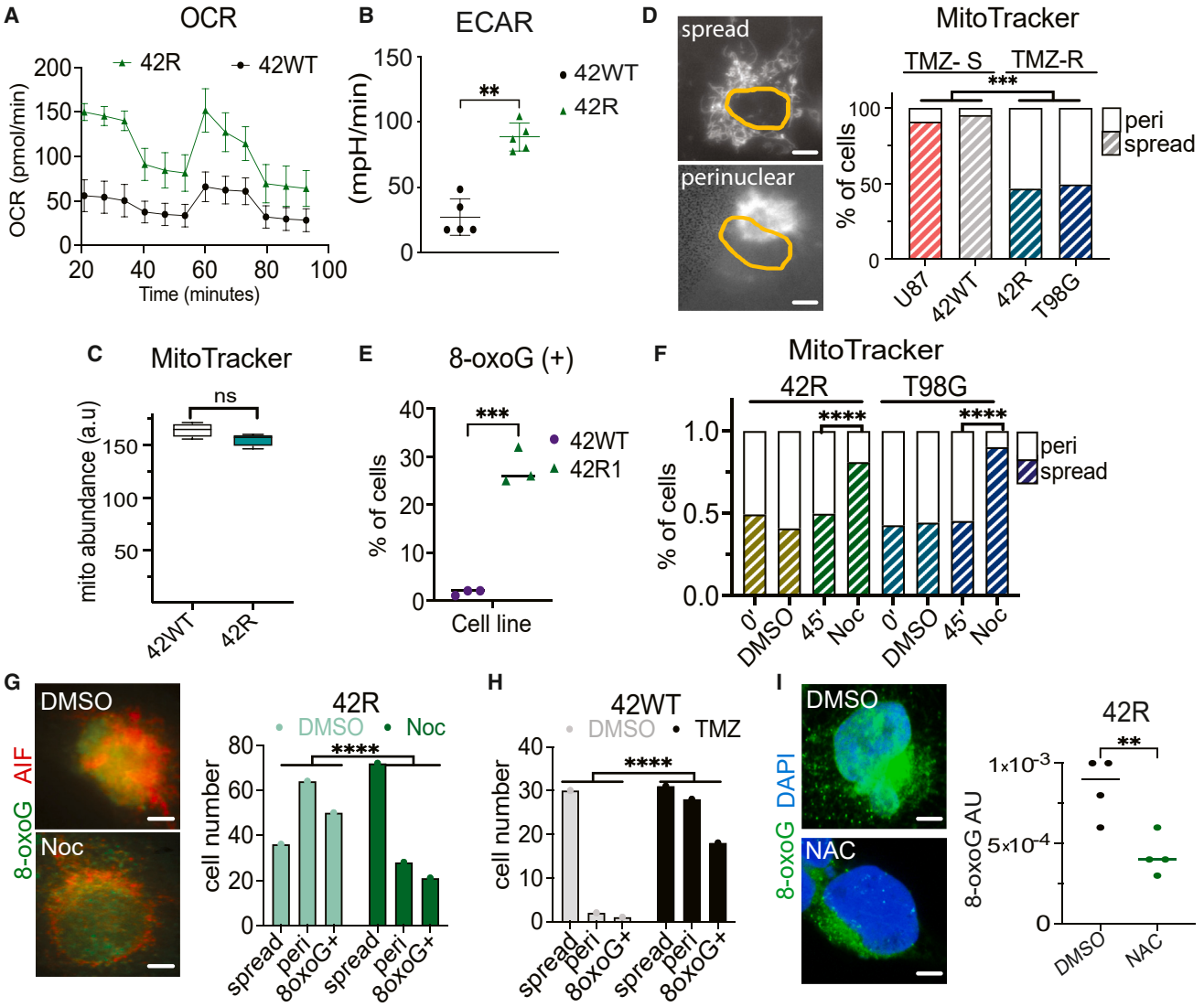

Figure 2. Mitochondria metabolism and location in TMZ-R GBM

(A) Seahorse mitochondria stress test in denoted cells treated with oligomycin, rotenone/antimycin A and FCCP at 40, 60, 80 min, respectively.

(B) Extracellular acidification rate (ECAR) determined from baseline reading from (A), t test.

(C) MitoTracker staining for 45 min (') in denoted cells.

(D) Left, representative live cell MitoTracker image where nucleus is outline in yellow. Right, quantification of mitochondria localization in denoted cells, perinuclear (peri) in stacked bars. Scale bar, 5 μm.

(E) IF quantification of cell percentage with 8-oxoG positive (+) staining, t test.

(F) MitoTracker staining of cells with 10 nM nocodazole (noc) or DMSO for 45 min (') one-way ANOVA.

(G) Left, representative images of 8-oxoG and AIF (mitochondria marker) IF with 45 min (') of DMSO or nocodazole (noc). Right, quantification of spread (cytoplasmic) and perinuclear (peri) mitochondria and the presence of nuclear 8-oxoG positive (+) cells, one-way ANOVA. Scale bar, 5 μm.

(H) Quantification of spread and perinuclear (peri) mitochondria and the presence of nuclear 8-oxoG positive (+) cells with 100 μM TMZ for 48 h.

(I) Left, representative IF image of 8-oxoG and DAPI (nuclear marker) with 6 h of DMSO or N-acetyl cysteine (NAC). Right, quantification 8-oxoG intensity, t test. Scale bar, 5 μm.

All error bars are SD; *$p < 0.05$, **$p < 0.001$, ***$p < 0.0005$, and ****$p < 0.0001$.

protein—EWSR1—of the FET (Fus, EWSR1, and Taf15) family specifically aggregates in TMZ-R GBM.[32] Immunofluorescent staining (IF) of pyroglutamic acid in GBM cells showed differential staining patterns between TMZ-S and -R lines with a diffuse cytoplasmic droplet-like staining in TMZ-S and more organized structures in TMZ-R lines (Figure 4A). A co-staining with EWSR1 showed some colocalization with pyroglutamic acid (Figure 4B), suggesting either aggregate binding or epitope masking. To confirm binding, we performed an immunoprecipitation (IP) for EWSR1 followed by immunoblotting (IB) for

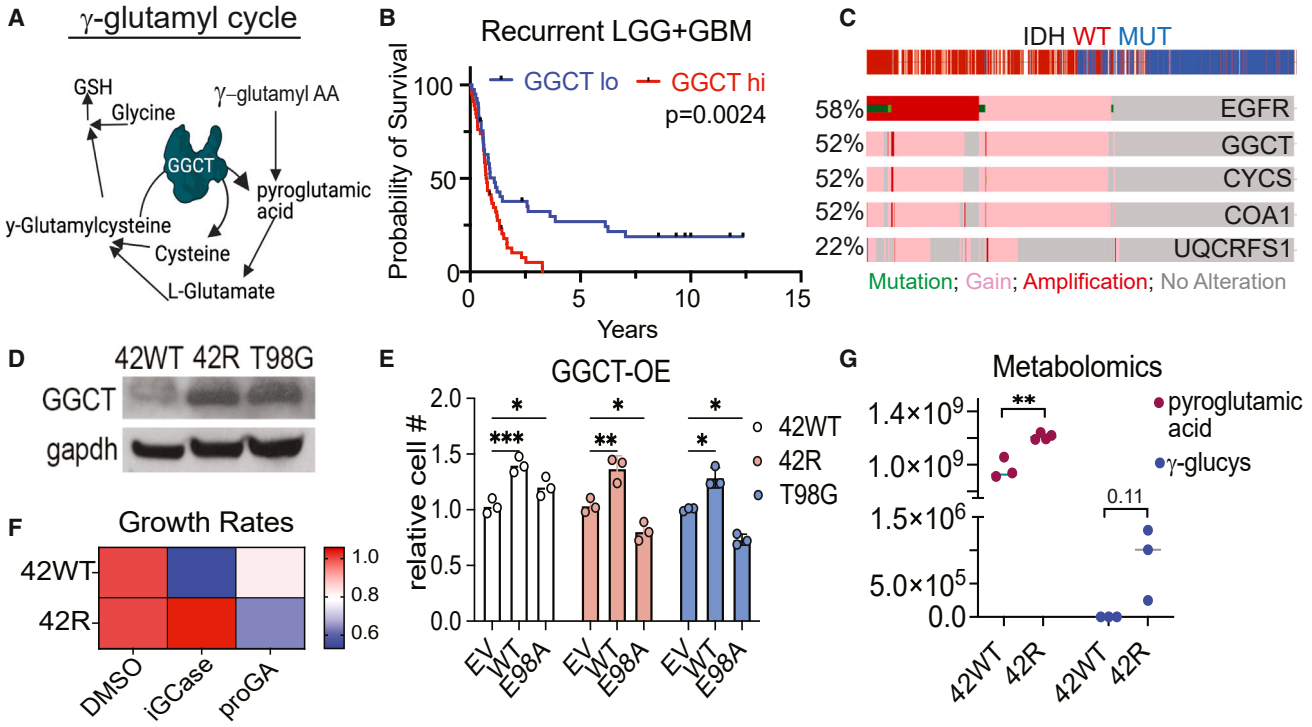

Figure 3. GGCT is overexpressed in TMZ-R GBM

(A) Cartoon of the dual role of GGCT in the γ-glutamyl pathway for glutathione (GSH) production.

(B) Kaplan-Meier plot for recurrent glioma delineated on GGCT expression from the CGGA dataset.

(C) CBioPortal data of genes gained, mutated, or amplified that are adjacent to EGFR on chromosome 7 involved in GSH production or mitochondria function.

(D) Immunoblot (IB) of GGCT in denoted cell lines.

(E) Cell titer glo assay for cell viability transfected with empty vector control (EV), GGCT wild type (WT), or GGCT catalytic mutant (E98A) one-way ANOVA.

(F) Cell titer glo assay for denoted cells treated with DMSO, iGCase, or iGGCT for 24 h.

(G) Metabolomics data from denoted cells quantifying pyroglutamic acid and γ-glutamylcysteine (γ-glucys) *t* Test. All error bars are SD; $^{*}p < 0.05$, $^{**}p < 0.001$, $^{***}p < 0.0005$, and $^{****}p < 0.0001$.

pyroglutamic acid where we observed two detectable protein species, one at ~95 kDa, the proposed molecular weight of EWSR1 protein, as well as a second protein species at ~180 kDa, representing a possible doublet of EWSR1 (Figure 4C). This binding along with the co-localization staining strengthens our hypothesis that pyroglutamic acid can bind to EWSR1 species.

In Alzheimer's disease, glutaminyl cyclase (QC) has been the focus to prevent intra-protein conversion of glutamate to pyroglutamic acid and affect protein seeding.[50] However, we tested the effect of inhibiting either GGCT (pro-GA[48]) or QC (PQ912[51]) and found that only GGCT inhibition decreased EWSR1 aggregates (Figure 4D). Accordingly, using our enzymatic mutant, we saw almost a complete loss of EWSR1 aggregation (Figure 4E). To link our observed phenotype back to the initial observation of increased oxidative stress, we hypothesized that only guanine-rich binding motif RNA binding proteins may be affected by the oxidative stress-induced 8-oxoG, and potentially affect RNA binding protein (RBP) binding. To test this, we induced oxidative stress with deferoxamine (DFO)[52] and performed IF on a cohort of RBPs and observed an increase in cytoplasmic localization specifically with G-rich binding RBPs, as compared to others (Figures 4F and 4G). Finally, as we had noted a band in our pyroglutamic input outside of EWSR1, we performed an IP assay for pyroglutamic acid followed by mass spectrometry and found the bound proteins enriched in pathways including protein refolding, substantia nigra development, and positive regulation of tau-protein kinase activity, among others (Table S1, list of proteomics hits from IP-mass spectrometry, related to Figure 4). These results strengthen our hypothesis that pyroglutamic acid can play a role in protein aggregation in brain disorders; however, more research is needed to conclusively determine the role of pyroglutamic acid in protein aggregation in other brain disorders.

Pyroglutamic acid binds EWSR1 in TMZ-R GBM patient samples

Finally, we sought to determine if this pathway of increased GGCT expression and pyroglutamic acid correlated with increased EWSR1 cytoplasmic aggregation in TMZ-R patient samples. Using nine matched pre- and post-treatment clinical GBM, IDH WT tumor samples (Table S2, related to Figure 5), we performed immunohistochemistry (IHC) staining for GGCT and EWSR1. We observed an increase in overall GGCT staining

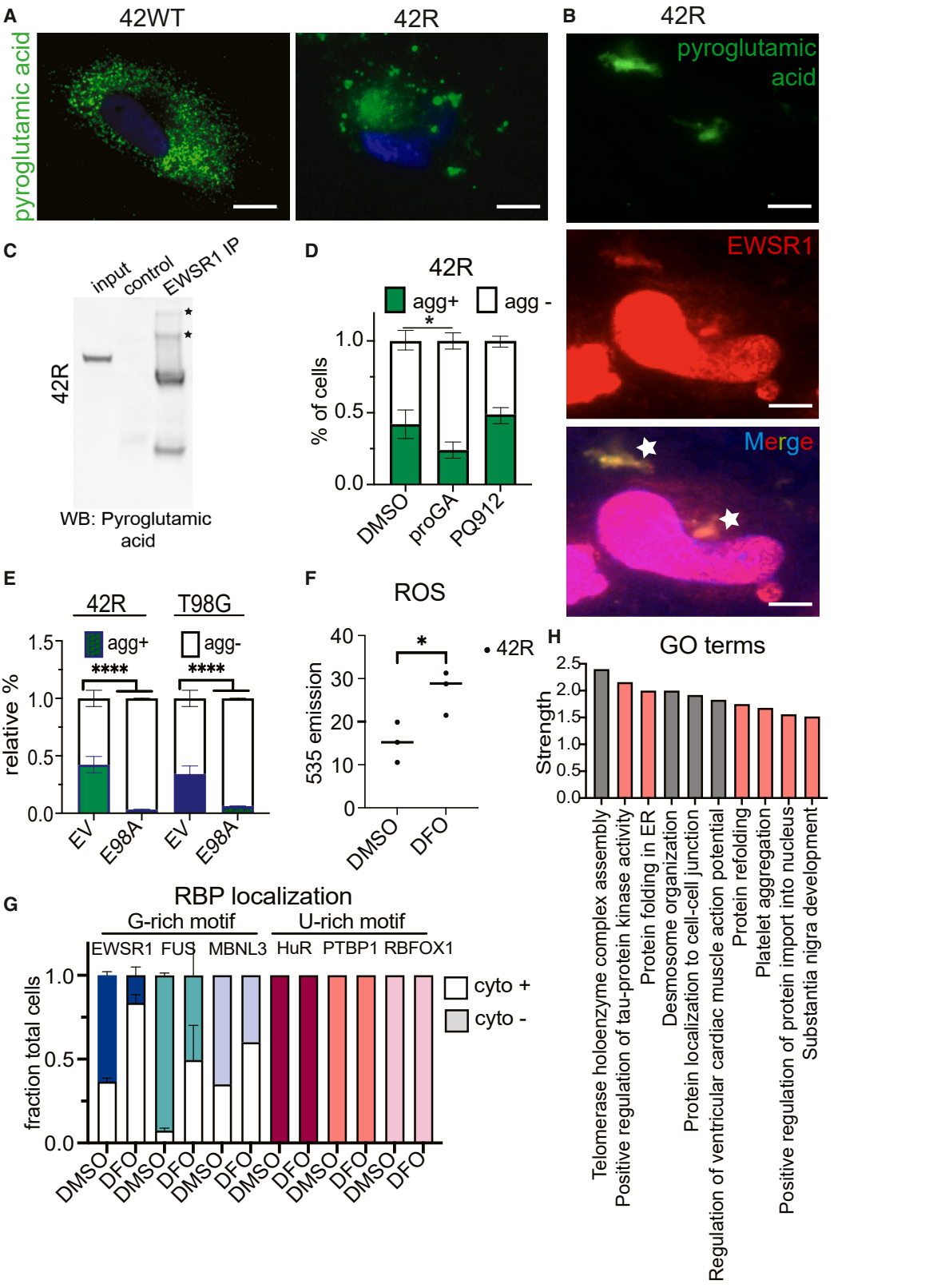

(legend on next page)

in the recurrent GBM tumors (Figures 5A and 5B), where we also detected an increase in EWSR1 cytoplasmic staining (Figures 5A and 5B). Finally, we stained for pyroglutamic acid and found that in an EWSR1 aggregate (−) sample, no pyroglutamic acid was observed, but in an EWSR1 aggregate (+) sample, the staining pattern of EWSR1 and pyroglutamic acid were similar within the cytoplasm (Figures 5A and 5B). Interestingly, we also observed an increase in EWSR1 aggregates in adjacent non-tumor brain from primary to recurrent samples (Figure 5C). In this way, these results suggest that in some recurrent GBMs this GGCT/pyroglutamic acid/EWSR1 signaling axis exists which may be used in the future to target these more oxidative metabolic tumors. When looking at the Online Mendelian Inheritance in Man (OMIM) database,[53] we found genetic changes in GGCT corresponded to diseases, such as ALS, bipolar disorder, Kuru, Parkinson's schizophrenia, and Creutzfeldt Jacob disease (CJD), among others (Figure 5D). Finally, we obtained four Alzheimer's disease (AD) samples and four cognitively normal (CN) samples (Table S3, related to Figure 5) and again performed IHC for EWSR1, GGCT, and pyroglutamic acid. Figure 5E shows representative images from two patients, where we found an increase in pyroglutamic acid staining in the AD brains—though you can see some staining in the CN brain that correlates to some EWSR1 cytoplasmic staining. However, there is a greater extent of EWSR1 and pyroglutamic acid in the cytoplasm in the AD brain compared to the CN elderly patient (Figure 5F). We also see an increase in GGCT staining in the AD brain (Figure 5F). Therefore, this pathway may also have the potential to lend insight into a different manner of protein aggregation in other neurological disorders in the future.

DISCUSSION

Aggregating proteins have been a hallmark of brain disorders and neurodegenerative diseases since Alois Alzheimer observed protein clumps in the brains of his patients afflicted with memory loss.[54] Today, this connection between aggregating proteins, like amyloid-beta, Tau, and Fus have been determined as diagnostic criteria through different imaging methods.[55] However, while these protein aggregates have dominated our cellular understanding of other brain disorders, the effect of these protein aggregates in brain cancers has been largely understudied. Here, we show that upon TMZ resistance, GBM cells now maintain a more oxidative state. This increase in oxidative stress is reminiscent of SOD1 or SOD2 mutations in Parkinson's disease or ALS disease where SOD1 mutation changes it from an antioxidant to a pro-oxidant enzyme and increases the ability of protein aggregates to be seeded.[18,56] We further show a role for both the mitochondria and its localization in promoting oxidative stress where TMZ-R GBM has increased mitochondrial function, but not mass, and where the perinuclear localization may allow for 8-oxo-G to affect the binding of G-rich sequence RNA binding proteins. Previous work has shown that 8-oxo-G bases allow for stronger HIF1A binding in hypoxic conditions broadly affecting gene expression, where movement of the mitochondria reduced 8-oxo-G abundance, HIF1A binding, and downstream gene expression suggesting an adaptive signaling role of 8-oxo-G.[38] However, the global effect of these oxidative stress marks warrants further investigation.

As we observed a dysregulated antioxidant response in these cells, we next queried the major antioxidant pathway, GSH, as this was also shown to be dysregulated in our metabolomics data—a caveat being the use of only cell lines. Previous work has shown that upon drug resistance, intertumoral pH can decrease as well as broad down regulation of antioxidant genes.[57] However, we found an increase in the GSH pathway enzyme GGCT. GGCT can play two distinct roles within the γ-glutamyl cycle to produce GSH. It can produce pyroglutamic acid (also known as 5-oxo-proline) as the first step in the pathway but can also hydrolyze the γ-glutamylcysteine intermediate to pyroglutamic acid and cysteine.[44] We hypothesized that this increase of pyroglutamic acid was occurring for a few reasons. First, GGCT is located on chromosome 7 which is commonly amplified in GBM,[45] allowing for more DNA copies and subsequent protein production of GGCT. There is also an increase in oxidative stress associated with drug treatments that in turn increase GSH production.[58] However, as has been previously shown in TMZ-R GBM there is a shift to *de novo* GTP production which requires glycine.[46] Therefore, if glycine is in lower supply to be used for GTP production, then the γ-glutamylcysteine intermediate which precedes glycine addition may have a longer half-life within the cell allowing GGCT hydrolysis. Other studies in prostate cancer have also shown increasing levels of GGCT expression correlate with lower overall survival, like we observe in both primary and recurrent gliomas.[59]

Lastly, as many metabolic products have been shown to affect protein aggregation, we propose GGCT-produced pyroglutamic acid is able to affect protein aggregation in TMZ-R GBM. In Alzheimer's disease, pyroglutamic acid with amyloid-beta has previously been shown to play a potential detrimental role.[60] This may be because the presence of pyroglutamic acid is indicative of a more oxidative environment which can have detrimental effects within the brain. We also show increased pyroglutamic acid IHC with EWSR1 aggregation in TMZ-R GBM patient samples,

Figure 4. Role of pyroglutamic acid and GGCT activity with cytoplasmic EWSR1

(A) IF of pyroglutamic acid in denoted cells. Scale bar, 5 μm.

(B) Co-stain of pyroglutamic acid and EWSR1 in 42R cells. Scale bar, 5 μm.

(C) Immunoprecipitation (IP) of EWSR1 followed by IB for pyroglutamic acid.

(D) Percentage (%) of cells with EWSR1 aggregates (agg) post 24 h treatment with proGA (iGGCT) or PQ912 (iGC), one-way ANOVA.

(E) Quantification of cells with EWSR1 aggregates (agg) transfected with control empty vector (EV) or GGCT catalytic mutant (E98A) one-way ANOVA.

(F) DCFDA quantification of ROS post 18 h treatment of deferoxamine (DFO), t test.

(G) IF of denoted RNA binding proteins with 18-h treatment of DFO.

(H) IP of pyroglutamic acid followed by mass spec analysis and gene ontology pathway analysis.

All error bars are SD; $^{*}p < 0.05$, $^{**}p < 0.001$, $^{***}p < 0.0005$, and $^{****}p < 0.0001$.

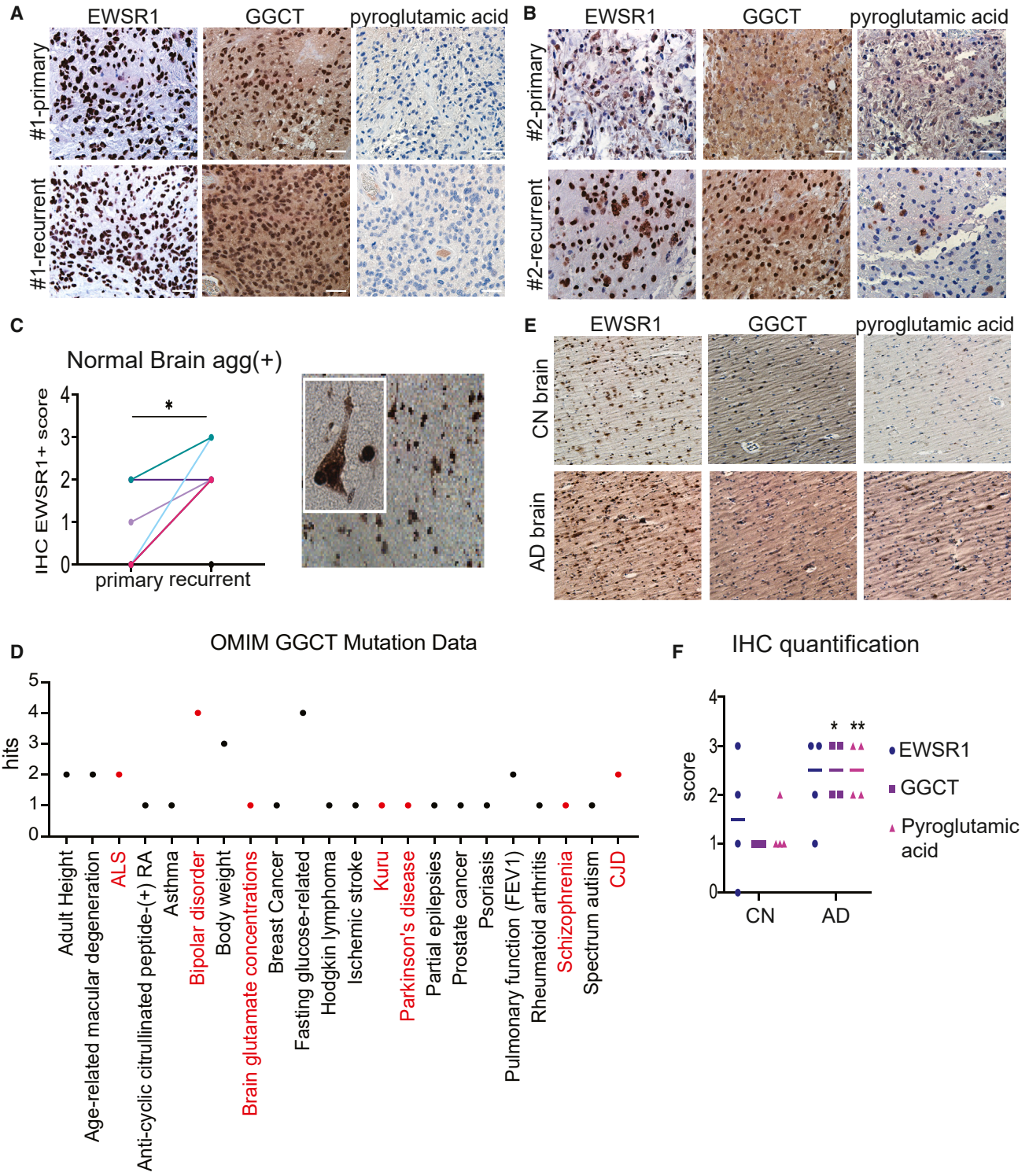

Figure 5. EWSR1 and pyroglutamic acid cytoplasmic localization in patient samples

(A and B) Immunohistochemistry (IHC) of representative matched primary and recurrent GBM patient samples (All IDH WT) of EWSR1, GGCT, and pyroglutamic acid with (A) EWSR1 aggregate (agg) negative (−) and (B) agg positive (+) (60X). Scale bar, 50 μm.

(C) EWSR1 IHC positive (+) normal brain in five matched patient samples with adjacent non-tumor brain, t test.

(legend continued on next page)

adjacent non-tumor brain, as well as AD brains as compared to CN brains. Others have also observed an increase of pyroglutamic acid in metabolomics data of TMZ-R versus -S samples,[61] and GGCT was shown to be one of the highest differentially expressed genes in an Alzheimer's patient cohort.[62] These data suggest further study of this pathway in other brain disorders.

In conclusion, we show that in our model of TMZ-R GBM we observe a dysregulated antioxidant response, changes in the mitochondria function, and localization that we suggest lead to increased GGCT-produced pyroglutamic acid that can lead to G-rich protein aggregation in the cytoplasm. We hypothesize that an increase of GGCT expression better allows for the degradation of γ-glutamylcysteine to pyroglutamic acid and cysteine. With the accumulation of pyroglutamic acid, this can then seed aggregation-prone proteins, like EWSR1. However, this seems to be restricted to TMZ-R models as they have increased oxidative stress, which would increase the production of γ-glutamylcysteine to create GSH. This oxidative stress pathway could lead to new therapeutic avenues for this deadly disease with protein aggregation or oxidative stress as a potential biomarker. Ultimately, further research into protein aggregation pathways in GBM could also lead to increasing our knowledge of protein aggregation in other brain disorders like neurodegenerative diseases and opening up new therapeutic avenues for disorders like Alzheimer's disease.

Limitations of the study

While we show that our endogenous cell models of protein aggregation are affected by oxidative stress and antioxidants, the study would be strengthened with more models and *in vivo* validation. As tracing pH *in vivo* can be technically challenging, we instead used patient samples from gliomas, Alzheimer's disease, and normal brains to show how changes in the GSH pathway correlate with protein aggregation. A larger patient cohort would also help in determining how prevalent this signaling axis is across other glioma patients.

RESOURCE AVAILABILITY

Lead contact

Further information and requests for resources and reagents should be directed to and will be fulfilled by the lead contact, Dr. Deanna Tiek (deanna.tiek@northwestern.edu).

Materials availability

This study did not generate new or unique reagents.

Data and code availability

- The proteomics data are attached as an Excel file as Table S1.
- No original code has been written for this manuscript.
- Any additional information required to analyze or questions associated with the data will be made available by the lead contact or contacting the co-corresponding authors.

ACKNOWLEDGMENTS

This work was supported by United States National Institutes of Health (NIH) grants, National Cancer Institute and Lou and Jean Malnati Brain Tumor Institute at Northwestern Medicine NS126810, NS125318, (S.-Y.C.); NCI CA234799 (D.T), CA279896 (D.T), United States Army Medical Research Acquisition Activity W81XWH-22-10373 (D.T.), W81XWH-22-1-0374 (X.S.). S.-Y.C. is a Zell Scholar at Northwestern University. The authors thank Northwestern University Feinberg School of Medicine Lurie Cancer Center Metabolomics Core and Northwestern Nervous System Tumor Bank (P50CA221747) and the Alzheimer's Disease Research Center (P30AG072977).

AUTHOR CONTRIBUTIONS

D.T. and S.-Y.C. conceived the project. D.T. performed almost all the experiments and X.S. performed computational analyses. C.H., A.C., K.M., and J.W. performed IHC staining and validation. R.C., R.V., and P.J. provided and analyzed AD samples. J.M. provided metabolism insight and experimental design. Manuscript writing – original Draft, D.T., X.S, S.-Y.C., and B.H.; Writing – Review & Editing, D.T, X.S, S.-Y.C., B.H., X.Y. Supervision, S.-Y.C. and B.H.; Project Administration, S.-Y.C. and B.H.; Funding Acquisition, D.T, S.-Y.C.

We support inclusive, diverse, and equitable conduct of research. One or more of the authors on this paper self-identifies as an underrepresented gender minority in science.

DECLARATION OF INTERESTS

The authors declare no competing interests.

STAR★METHODS

Detailed methods are provided in the online version of this paper and include the following:

- KEY RESOURCES TABLE
- EXPERIMENTAL MODEL AND STUDY PARTICIPANT DETAILS
  - Cell lines and cell culture
  - Study approval
  - Sex as a biological variable
- METHOD DETAILS
  - pH measurements intracellular and extracellular
  - Metabolomics analysis
  - *In vitro* cell growth assays
  - Oxygen consumption rate and extracellular acidification rate
  - MitoTracker mitochondrial mass and imaging assay
  - Immunofluorescence assays
  - Immunoblot and immunoprecipitation analysis
  - ROS detection
  - Gene expression analysis in glioma single cell (sc)RNA-seq dataset
  - Immunohistochemistry (IHC) analysis
- QUANTIFICATION AND STATISTICAL ANALYSIS
  - Statistical analysis
  - Data availability

SUPPLEMENTAL INFORMATION

Supplemental information can be found online at https://doi.org/10.1016/j.isci.2025.111769.

(D) OMIM GGCT mutation data corresponding to the denoted diseased state.
(E) IHC of representative Alzheimer's disease (AD, case #2) and cognitive normal (CN, case #6) patient brains of pyroglutamic acid, EWSR1, and GGCT (60X).
(F) Quantification of IHC from (E) t test.
All error bars are SD; $*p < 0.05$, $**p < 0.001$, $***p < 0.0005$, and $****p < 0.0001$.

Received: June 26, 2024
Revised: September 13, 2024
Accepted: January 6, 2025
Published: January 7, 2025

REFERENCES

1. Ross, C.A., and Poirier, M.A. (2004). Protein aggregation and neurodegenerative disease. Nat. Med. *10*, S10–S17. https://doi.org/10.1038/nm1066.
2. Hedna, R., Kovacic, H., Pagano, A., Peyrot, V., Robin, M., Devred, F., and Breuzard, G. (2022). Tau Protein as Therapeutic Target for Cancer? Focus on Glioblastoma. Cancers *14*, 5386. https://doi.org/10.3390/cancers14215386.
3. Stupp, R., Taillibert, S., Kanner, A., Read, W., Steinberg, D., Lhermitte, B., Toms, S., Idbaih, A., Ahluwalia, M.S., Fink, K., et al. (2017). Effect of Tumor-Treating Fields Plus Maintenance Temozolomide vs Maintenance Temozolomide Alone on Survival in Patients With Glioblastoma: A Randomized Clinical Trial. JAMA *318*, 2306–2316. https://doi.org/10.1001/jama.2017.18718.
4. Stupp, R., Mason, W.P., Van den Bent, M.J., Weller, M., Fisher, B., Taphoorn, M.J.B., Belanger, K., Brandes, A.A., Marosi, C., Bogdahn, U., et al. (2005). Radiotherapy plus concomitant and adjuvant temozolomide for glioblastoma. N. Engl. J. Med. *352*, 987–996. https://doi.org/10.1056/NEJMoa043330.
5. Singh, N., Miner, A., Hennis, L., and Mittal, S. (2021). Mechanisms of temozolomide resistance in glioblastoma - a comprehensive review. Cancer Drug Resist. *4*, 17–43. https://doi.org/10.20517/cdr.2020.79.
6. Oren, Y., Tsabar, M., Cuoco, M.S., Amir-Zilberstein, L., Cabanos, H.F., Hütter, J.C., Hu, B., Thakore, P.I., Tabaka, M., Fulco, C.P., et al. (2021). Cycling cancer persister cells arise from lineages with distinct programs. Nature *596*, 576–582. https://doi.org/10.1038/s41586-021-03796-6.
7. Hangauer, M.J., Viswanathan, V.S., Ryan, M.J., Bole, D., Eaton, J.K., Matov, A., Galeas, J., Dhruv, H.D., Berens, M.E., Schreiber, S.L., et al. (2017). Drug-tolerant persister cancer cells are vulnerable to GPX4 inhibition. Nature *551*, 247–250. https://doi.org/10.1038/nature24297.
8. Harris, I.S., Treloar, A.E., Inoue, S., Sasaki, M., Gorrini, C., Lee, K.C., Yung, K.Y., Brenner, D., Knobbe-Thomsen, C.B., Cox, M.A., et al. (2015). Glutathione and thioredoxin antioxidant pathways synergize to drive cancer initiation and progression. Cancer Cell *27*, 211–222. https://doi.org/10.1016/j.ccell.2014.11.019.
9. Meister, A. (1988). Glutathione metabolism and its selective modification. J. Biol. Chem. *263*, 17205–17208.
10. Kussmaul, L., and Hirst, J. (2006). The mechanism of superoxide production by NADH:ubiquinone oxidoreductase (complex I) from bovine heart mitochondria. Proc. Natl. Acad. Sci. USA *103*, 7607–7612. https://doi.org/10.1073/pnas.0510977103.
11. Guzy, R.D., Hoyos, B., Robin, E., Chen, H., Liu, L., Mansfield, K.D., Simon, M.C., Hammerling, U., and Schumacker, P.T. (2005). Mitochondrial complex III is required for hypoxia-induced ROS production and cellular oxygen sensing. Cell Metab. *1*, 401–408. https://doi.org/10.1016/j.cmet.2005.05.001.
12. Diehn, M., Cho, R.W., Lobo, N.A., Kalisky, T., Dorie, M.J., Kulp, A.N., Qian, D., Lam, J.S., Ailles, L.E., Wong, M., et al. (2009). Association of reactive oxygen species levels and radioresistance in cancer stem cells. Nature *458*, 780–783. https://doi.org/10.1038/nature07733.
13. Perillo, B., Di Donato, M., Pezone, A., Di Zazzo, E., Giovannelli, P., Galasso, G., Castoria, G., and Migliaccio, A. (2020). ROS in cancer therapy: the bright side of the moon. Exp. Mol. Med. *52*, 192–203. https://doi.org/10.1038/s12276-020-0384-2.
14. Rink, C., and Khanna, S. (2011). Significance of brain tissue oxygenation and the arachidonic acid cascade in stroke. Antioxid. Redox Signal. *14*, 1889–1903. https://doi.org/10.1089/ars.2010.3474.
15. Siddique, T., and Deng, H.X. (1996). Genetics of amyotrophic lateral sclerosis. Hum. Mol. Genet. *5*, 1465–1470. https://doi.org/10.1093/hmg/5.supplement_1.1465.
16. Mattiazzi, M., D'Aurelio, M., Gajewski, C.D., Martushova, K., Kiaei, M., Beal, M.F., and Manfredi, G. (2002). Mutated human SOD1 causes dysfunction of oxidative phosphorylation in mitochondria of transgenic mice. J. Biol. Chem. *277*, 29626–29633. https://doi.org/10.1074/jbc.M203065200.
17. Ghadge, G.D., Lee, J.P., Bindokas, V.P., Jordan, J., Ma, L., Miller, R.J., and Roos, R.P. (1997). Mutant superoxide dismutase-1-linked familial amyotrophic lateral sclerosis: molecular mechanisms of neuronal death and protection. J. Neurosci. *17*, 8756–8766. https://doi.org/10.1523/JNEUROSCI.17-22-08756.1997.
18. Bakavayev, S., Chetrit, N., Zvagelsky, T., Mansour, R., Vyazmensky, M., Barak, Z., Israelson, A., and Engel, S. (2019). Cu/Zn-superoxide dismutase and wild-type like fALS SOD1 mutants produce cytotoxic quantities of H(2)O(2) via cysteine-dependent redox short-circuit. Sci. Rep. *9*, 10826. https://doi.org/10.1038/s41598-019-47326-x.
19. Shaham-Niv, S., Adler-Abramovich, L., Schnaider, L., and Gazit, E. (2015). Extension of the generic amyloid hypothesis to nonproteinaceous metabolite assemblies. Sci. Adv. *1*, e1500137. https://doi.org/10.1126/sciadv.1500137.
20. Adler-Abramovich, L., Vaks, L., Carny, O., Trudler, D., Magno, A., Caflisch, A., Frenkel, D., and Gazit, E. (2012). Phenylalanine assembly into toxic fibrils suggests amyloid etiology in phenylketonuria. Nat. Chem. Biol. *8*, 701–706. https://doi.org/10.1038/nchembio.1002.
21. Tavassoly, O., Sade, D., Bera, S., Shaham-Niv, S., Vocadlo, D.J., and Gazit, E. (2018). Quinolinic Acid Amyloid-like Fibrillar Assemblies Seed alpha-Synuclein Aggregation. J. Mol. Biol. *430*, 3847–3862. https://doi.org/10.1016/j.jmb.2018.08.002.
22. Kam, T.I., Mao, X., Park, H., Chou, S.C., Karuppagounder, S.S., Umanah, G.E., Yun, S.P., Brahmachari, S., Panicker, N., Chen, R., et al. (2018). Poly(ADP-ribose) drives pathologic alpha-synuclein neurodegeneration in Parkinson's disease. Science *362*, eaat8407. https://doi.org/10.1126/science.aat8407.
23. Gunn, A.P., Wong, B.X., McLean, C., Fowler, C., Barnard, P.J., Duce, J.A., and Roberts, B.R.; AIBL Research Group (2021). Increased glutaminyl cyclase activity in brains of Alzheimer's disease individuals. J. Neurochem. *156*, 979–987. https://doi.org/10.1111/jnc.15114.
24. Vasan, N., Baselga, J., and Hyman, D.M. (2019). A view on drug resistance in cancer. Nature *575*, 299–309. https://doi.org/10.1038/s41586-019-1730-1.
25. Tiek, D.M., Rone, J.D., Graham, G.T., Pannkuk, E.L., Haddad, B.R., and Riggins, R.B. (2018). Alterations in Cell Motility, Proliferation, and Metabolism in Novel Models of Acquired Temozolomide Resistant Glioblastoma. Sci. Rep. *8*, 7222. https://doi.org/10.1038/s41598-018-25588-1.
26. Maulucci, G., Chiarpotto, M., Papi, M., Samengo, D., Pani, G., and De Spirito, M. (2015). Quantitative analysis of autophagic flux by confocal pH-imaging of autophagic intermediates. Autophagy *11*, 1905–1916. https://doi.org/10.1080/15548627.2015.1084455.
27. Shi, D.D., Savani, M.R., Levitt, M.M., Wang, A.C., Endress, J.E., Bird, C.E., Buehler, J., Stopka, S.A., Regan, M.S., Lin, Y.F., et al. (2022). De novo pyrimidine synthesis is a targetable vulnerability in IDH mutant glioma. Cancer Cell *40*, 939–956.e16. https://doi.org/10.1016/j.ccell.2022.07.011.
28. Pal, S., Kaplan, J.P., Nguyen, H., Stopka, S.A., Savani, M.R., Regan, M.S., Nguyen, Q.D., Jones, K.L., Moreau, L.A., Peng, J., et al. (2022). A druggable addiction to de novo pyrimidine biosynthesis in diffuse midline glioma. Cancer Cell *40*, 957–972.e10. https://doi.org/10.1016/j.ccell.2022.07.012.
29. Perrault, E.N., Shireman, J.M., Ali, E.S., Lin, P., Preddy, I., Park, C., Budhiraja, S., Baisiwala, S., Dixit, K., James, C.D., et al. (2023). Ribonucleotide reductase regulatory subunit M2 drives glioblastoma TMZ resistance through modulation of dNTP production. Sci. Adv. *9*, eade7236. https://doi.org/10.1126/sciadv.ade7236.

30. Niu, B., Liao, K., Zhou, Y., Wen, T., Quan, G., Pan, X., and Wu, C. (2021). Application of glutathione depletion in cancer therapy: Enhanced ROS-based therapy, ferroptosis, and chemotherapy. Biomaterials *277*, 121110. https://doi.org/10.1016/j.biomaterials.2021.121110.

31. Levy, E., El Banna, N., Baille, D., Heneman-Masurel, A., Truchet, S., Rezaei, H., Huang, M.E., Beringue, V., Martin, D., and Vernis, L. (2019). Causative Links between Protein Aggregation and Oxidative Stress: A Review. Int. J. Mol. Sci. *20*, 3896. https://doi.org/10.3390/ijms20163896.

32. Tiek, D.M., Erdogdu, B., Razaghi, R., Jin, L., Sadowski, N., Alamillo-Ferrer, C., Hogg, J.R., Haddad, B.R., Drewry, D.H., Wells, C.I., et al. (2022). Temozolomide-induced guanine mutations create exploitable vulnerabilities of guanine-rich DNA and RNA regions in drug-resistant gliomas. Sci. Adv. *8*, eabn3471. https://doi.org/10.1126/sciadv.abn3471.

33. Zhitkovich, A. (2019). N-Acetylcysteine: Antioxidant, Aldehyde Scavenger, and More. Chem. Res. Toxicol. *32*, 1318–1319. https://doi.org/10.1021/acs.chemrestox.9b00152.

34. Turrens, J.F. (2003). Mitochondrial formation of reactive oxygen species. J. Physiol. *552*, 335–344. https://doi.org/10.1113/jphysiol.2003.049478.

35. Gu, X., Ma, Y., Liu, Y., and Wan, Q. (2021). Measurement of mitochondrial respiration in adherent cells by Seahorse XF96 Cell Mito Stress Test. STAR Protoc. *2*, 100245. https://doi.org/10.1016/j.xpro.2020.100245.

36. Chazotte, B. (2011). Labeling mitochondria with MitoTracker dyes. Cold Spring Harb. Protoc. *2011*, 990–992. https://doi.org/10.1101/pdb.prot5648.

37. Chiorcea-Paquim, A.M. (2022). 8-oxoguanine and 8-oxodeoxyguanosine Biomarkers of Oxidative DNA Damage: A Review on HPLC-ECD Determination. Molecules *27*, 1620. https://doi.org/10.3390/molecules27051620.

38. Al-Mehdi, A.-B., Pastukh, V.M., Swiger, B.M., Reed, D.J., Patel, M.R., Bardwell, G.C., Pastukh, V.V., Alexeyev, M.F., and Gillespie, M.N. (2012). Perinuclear mitochondrial clustering creates an oxidant-rich nuclear domain required for hypoxia-induced transcription. Sci. Signal. *5*, ra47. https://doi.org/10.1126/scisignal.2002712.

39. Orlowski, M., and Meister, A. (1970). The gamma-glutamyl cycle: a possible transport system for amino acids. Proc. Natl. Acad. Sci. USA *67*, 1248–1255. https://doi.org/10.1073/pnas.67.3.1248.

40. Van der Werf, P., Orlowski, M., and Meister, A. (1971). Enzymatic conversion of 5-oxo-L-proline (L-pyrrolidone carboxylate) to L-glutamate coupled with cleavage of adenosine triphosphate to adenosine diphosphate, a reaction in the -glutamyl cycle. Proc. Natl. Acad. Sci. USA *68*, 2982–2985. https://doi.org/10.1073/pnas.68.12.2982.

41. Cancer Genome Atlas Research Network; Weinstein, J.N., Collisson, E.A., Mills, G.B., Shaw, K.R.M., Ozenberger, B.A., Ellrott, K., Shmulevich, I., Sander, C., and Stuart, J.M. (2013). The Cancer Genome Atlas Pan-Cancer analysis project. Nat. Genet. *45*, 1113–1120. https://doi.org/10.1038/ng.2764.

42. Zhao, Z., Zhang, K.N., Wang, Q., Li, G., Zeng, F., Zhang, Y., Wu, F., Chai, R., Wang, Z., Zhang, C., et al. (2021). Chinese Glioma Genome Atlas (CGGA): A Comprehensive Resource with Functional Genomic Data from Chinese Glioma Patients. Dev. Reprod. Biol. *19*, 1–12. https://doi.org/10.1016/j.gpb.2020.10.005.

43. Gusev, Y., Bhuvaneshwar, K., Song, L., Zenklusen, J.C., Fine, H., and Madhavan, S. (2018). The REMBRANDT study, a large collection of genomic data from brain cancer patients. Sci. Data *5*, 180158. https://doi.org/10.1038/sdata.2018.158.

44. Oakley, A.J., Yamada, T., Liu, D., Coggan, M., Clark, A.G., and Board, P.G. (2008). The identification and structural characterization of C7orf24 as gamma-glutamyl cyclotransferase. An essential enzyme in the gamma-glutamyl cycle. J. Biol. Chem. *283*, 22031–22042. https://doi.org/10.1074/jbc.M803623200.

45. Louis, D.N., Perry, A., Wesseling, P., Brat, D.J., Cree, I.A., Figarella-Branger, D., Hawkins, C., Ng, H.K., Pfister, S.M., Reifenberger, G., et al. (2021). The 2021 WHO Classification of Tumors of the Central Nervous System: a summary. Neuro Oncol. *23*, 1231–1251. https://doi.org/10.1093/neuonc/noab106.

46. Shireman, J.M., Atashi, F., Lee, G., Ali, E.S., Saathoff, M.R., Park, C.H., Savchuk, S., Baisiwala, S., Miska, J., Lesniak, M.S., et al. (2021). De novo purine biosynthesis is a major driver of chemoresistance in glioblastoma. Brain *144*, 1230–1246. https://doi.org/10.1093/brain/awab020.

47. Chen, T.S., Richie, J.P., Nagasawa, H.T., and Lang, C.A. (2000). Glutathione monoethyl ester protects against glutathione deficiencies due to aging and acetaminophen in mice. Mech. Ageing Dev. *120*, 127–139. https://doi.org/10.1016/s0047-6374(00)00214-1.

48. Hanada, E., Kageyama, S., Murai, R., Kubota, S., Ii, H., Nakata, S., Kita, H., Kawauchi, A., and Chano, T. (2019). Pro-GA, a Novel Inhibitor of gamma-Glutamylcyclotransferase, Suppresses Human Bladder Cancer Cell Growth. Anticancer Res. *39*, 1893–1898. https://doi.org/10.21873/anticanres.13297.

49. Schlenzig, D., Manhart, S., Cinar, Y., Kleinschmidt, M., Hause, G., Willbold, D., Funke, S.A., Schilling, S., and Demuth, H.U. (2009). Pyroglutamate Formation Influences Solubility and Amyloidogenicity of Amyloid Peptides. Biochemistry *48*, 7072–7078. https://doi.org/10.1021/bi900818a.

50. Scheltens, P., Hallikainen, M., Grimmer, T., Duning, T., Gouw, A.A., Teunissen, C.E., Wink, A.M., Maruff, P., Harrison, J., van Baal, C.M., et al. (2018). Safety, tolerability and efficacy of the glutaminyl cyclase inhibitor PQ912 in Alzheimer's disease: results of a randomized, double-blind, placebo-controlled phase 2a study. Alzheimers Res. Ther. *10*, 107. https://doi.org/10.1186/s13195-018-0431-6.

51. Hoffmann, T., Meyer, A., Heiser, U., Kurat, S., Böhme, L., Kleinschmidt, M., Bühring, K.U., Hutter-Paier, B., Farcher, M., Demuth, H.U., et al. (2017). Glutaminyl Cyclase Inhibitor PQ912 Improves Cognition in Mouse Models of Alzheimer's Disease-Studies on Relation to Effective Target Occupancy. J. Pharmacol. Exp. Therapeut. *362*, 119–130. https://doi.org/10.1124/jpet.117.240614.

52. Liu, Y., Cui, Y., Shi, M., Zhang, Q., Wang, Q., and Chen, X. (2014). Deferoxamine promotes MDA-MB-231 cell migration and invasion through increased ROS-dependent HIF-1alpha accumulation. Cell. Physiol. Biochem. *33*, 1036–1046. https://doi.org/10.1159/000358674.

53. Amberger, J.S., Bocchini, C.A., Schiettecatte, F., Scott, A.F., and Hamosh, A. (2015). OMIM.org: Online Mendelian Inheritance in Man (OMIM(R)), an online catalog of human genes and genetic disorders. Nucleic Acids Res. *43*, D789–D798. https://doi.org/10.1093/nar/gku1205.

54. Hippius, H., and Neundörfer, G. (2003). The discovery of Alzheimer's disease. Dialogues Clin. Neurosci. *5*, 101–108. https://doi.org/10.31887/DCNS.2003.5.1/hhippius.

55. De, S., and Klenerman, D. (2019). Imaging individual protein aggregates to follow aggregation and determine the role of aggregates in neurodegenerative disease. Biochim. Biophys. Acta, Proteins Proteomics *1867*, 870–878. https://doi.org/10.1016/j.bbapap.2018.12.010.

56. Rosen, D.R., Siddique, T., Patterson, D., Figlewicz, D.A., Sapp, P., Hentati, A., Donaldson, D., Goto, J., O'Regan, J.P., Deng, H.X., et al. (1993). Mutations in Cu/Zn superoxide dismutase gene are associated with familial amyotrophic lateral sclerosis. Nature *362*, 59–62. https://doi.org/10.1038/362059a0.

57. Tiek, D., and Cheng, S.Y. (2022). DNA damage and metabolic mechanisms of cancer drug resistance. Cancer Drug Resist. *5*, 368–379. https://doi.org/10.20517/cdr.2021.148.

58. Lu, H., Samanta, D., Xiang, L., Zhang, H., Hu, H., Chen, I., Bullen, J.W., and Semenza, G.L. (2015). Chemotherapy triggers HIF-1-dependent glutathione synthesis and copper chelation that induces the breast cancer stem cell phenotype. Proc. Natl. Acad. Sci. USA *112*, E4600–E4609. https://doi.org/10.1073/pnas.1513433112.

59. Ii, H., Yoshiya, T., Nakata, S., Taniguchi, K., Hidaka, K., Tsuda, S., Mochizuki, M., Nishiuchi, Y., Tsuda, Y., Ito, K., et al. (2018). A Novel Prodrug of a γ-Glutamylcyclotransferase Inhibitor Suppresses Cancer Cell Proliferation in vitro and Inhibits Tumor Growth in a Xenograft Mouse Model of Prostate

Cancer. ChemMedChem *13*, 155–163. https://doi.org/10.1002/cmdc.201700660.

60. Jawhar, S., Wirths, O., and Bayer, T.A. (2011). Pyroglutamate amyloid-beta (Abeta): a hatchet man in Alzheimer disease. J. Biol. Chem. *286*, 38825–38832. https://doi.org/10.1074/jbc.R111.288308.

61. Zhao, H., Heimberger, A.B., Lu, Z., Wu, X., Hodges, T.R., Song, R., and Shen, J. (2016). Metabolomics profiling in plasma samples from glioma patients correlates with tumor phenotypes. Oncotarget *7*, 20486–20495. https://doi.org/10.18632/oncotarget.7974.

62. Higginbotham, L., Ping, L., Dammer, E.B., Duong, D.M., Zhou, M., Gearing, M., Hurst, C., Glass, J.D., Factor, S.A., Johnson, E.C.B., et al. (2020). Integrated proteomics reveals brain-based cerebrospinal fluid biomarkers in asymptomatic and symptomatic Alzheimer's disease. Sci. Adv. *6*, eaaz9360. https://doi.org/10.1126/sciadv.aaz9360.

63. Chaligne, R., Gaiti, F., Silverbush, D., Schiffman, J.S., Weisman, H.R., Kluegel, L., Gritsch, S., Deochand, S.D., Gonzalez Castro, L.N., Richman, A.R., et al. (2021). Epigenetic encoding, heritability and plasticity of glioma transcriptional cell states. Nat. Genet. *53*, 1469–1479. https://doi.org/10.1038/s41588-021-00927-7.

STAR★METHODS

KEY RESOURCES TABLE

REAGENT or RESOURCE	SOURCE	IDENTIFIER
Antibodies		
EWSR1 rabbit	Abcam ab133288	
EWSR1 mouse	SCBT sc-48404	
Alexa Flour 488 mouse	Life Technologies A11029	
Alexa Flour 594 rabbit	Life Technologies A11037	
GGCT rabbit	Proteintech 16257-1-AP	
Pyroglutamic acid	LSBio LS-C664190	
Biological samples		
Glioblastoma patient samples	Nervous System Tumor Bank - Northwestern	
Alzheimer's patient samples	Alzheimer's Disease Research Center - Northwestern	
Chemicals, peptides, and recombinant proteins		
Fluoro-Gel	Electron Microscopy Sciences 17985-30	
Horseradish peroxidase	Promega W4028,W2018	
Chemiluminescence	Cytiva RPN2106V1	
Critical commercial assays		
VenorGeM Mycoplasma Detection Kit	Sigma-Aldrich, MP0025	
pHrodo Red AM Intracellular pH	Life Technologies, P35372	
CellTiter-Glo Luminescent Cell Vilability Kit	Promega	
Seahorse XF Mito Stress Test Kit	Agilent; 103015-100	
MitoTracker Green FM	Thermo M7514	
Experimental models: Cell lines		
42MGBA	Georgetown University	
42MGBA-TMZR	Georgetown University	
8MGBA	Georgetown University	
8MBGA-TMZR	Georgetown University	
U87-MG	Northwestern University	
T98G	Northwestern University	
U118-MG	Northwestern University	
Recombinant DNA		
GGCT-WT Plasmid	Kind gift from Phillip Board	
GGCT-E98A Plasmid	Kind gift from Phillip Board	
GGCT-E98Q Plasmid	Kind gift from Phillip Board	
Software and algorithms		
Prism 10	Northwestern University	
Xcalibur 4.1	Thermo Fisher	
Tracefinder 4.1	Thermo Fisher	
Fisher Scientific Accumet AE150	Fisher Scientific	

EXPERIMENTAL MODEL AND STUDY PARTICIPANT DETAILS

Cell lines and cell culture

Patient-derived isogenic TMZ-sensitive 42MGBA-WT, 8MGBA-WT, and TMZ-R 42MGBA-R, 8MGBA-R[25] and GBM U87, U251, T98G, U118-MG cells were cultured in DMEM (Thermo Fisher Scientific, 11995-065) supplemented with 10% FBS (Thermo Fisher Scientific, 10437028.) All the GBM cell lines were authenticated by short tandem repeat analysis at IDEXX BioAnalytics, Texas Tech University Health Sciences Center (Lubbock, TX), or Northwestern University NUSeq core facility. All cell lines were tested

negative for Mycoplasma using VenorGeM Mycoplasma Detection Kit (Sigma-Aldrich, MP0025). The latest authentication and Mycoplasma testing were in December 2022. All cell lines were cultured less than 15 passages prior to use.

Study approval

All Human Subjects research protocols were approved by the Northwestern Institutional Review Board and deidentified patient samples were shared for research purposes. All studies were done in accordance with the guidelines from the Declaration of Helsinki, NIH, and Northwestern's Ethics Committee. Glioma specimens and the Alzheimer's Disease patient brain genetics, age, sex, diagnosis, and other relevant information are in Tables S2 and S3, respectively. In total, 9 GBM patient samples were used – primary and recurrent – with 18 samples for this analysis. For the AD cases, 4 AD brains and 4 cognitive normal brains were used for analysis.

Sex as a biological variable

Our study examined patient data of both male and females and similar findings were found for both sexes.

METHOD DETAILS

pH measurements intracellular and extracellular

Cells were seeded in 96-well plates (Falcon; 353072) at 5,000 cells/well and allowed to attach overnight. The next day cells were stained with pHrodo Red AM Intracellular pH indicator (Life Technologies; P35372) per manufacturer's instructions at room temperature for 30 min. Fluorescent intensity was read at 560/585 on a Spectra Max3 immediately following the staining. For extracellular media pH reading, cells were seeded in 10 cm plates at $1e^6$ cells/plate. Conditioned media was collected 48 h later, and pH was determined via Fisher Scientific accumet AE150.

Metabolomics analysis

Designated cells were grown where 3 replicates of $1e^6$ cells were pelleted and frozen at −80°C. Extraction solution was dried using SpeedVac. 60% acetonitrile was added to the tube for reconstitution following by overtaxing for 30 s. Sample solution was then centrifuged for 30 min @ 20,000g, at 4°C. Supernatant was collected for LCMS analysis.

Samples were analyzed at NU Feinberg Proteomics Core by High-Performance Liquid Chromatography and High-Resolution Mass Spectrometry and Tandem Mass Spectrometry (HPLC-MS/MS). Specifically, the system consisted of a Thermo Q-Exactive in line with an electrospray source and an Ultimate3000 (Thermo) series HPLC consisting of a binary pump, degasser, and autosampler outfitted with a Xbridge Amide column (Waters; dimensions of 3.0 mm × 100 mm and a 3.5 μm particle size). The mobile phase A contained 95% (vol/vol) water, 5% (vol/vol) acetonitrile, 10 mM ammonium hydroxide, 10 mM ammonium acetate, pH = 9.0; B was 100% Acetonitrile. The gradient was as following: 0 min, 15% A; 2.5 min, 30% A; 7 min, 43% A; 16 min, 62% A; 16.1–18 min, 75% A; 18–25 min, 15% A with a flow rate of 150 μL/min. The capillary of the ESI source was set to 275°C, with sheath gas at 35 arbitrary units, auxiliary gas at 5 arbitrary units and the spray voltage at 4.0 kV. In positive/negative polarity switching mode, an *m/z* scan range from 60 to 900 was chosen and MS1 data was collected at a resolution of 70,000. The automatic gain control (AGC) target was set at 1×10^6 and the maximum injection time was 200 m. The top 5 precursor ions were subsequently fragmented, in a data-dependent manner, using the higher energy collisional dissociation (HCD) cell set to 30% normalized collision energy in MS2 at a resolution power of 17,500. Besides matching m/z, metabolites are identified by matching either retention time with analytical standards and/or MS2 fragmentation pattern. Data acquisition and analysis were carried out by Xcalibur 4.1 software and Tracefinder 4.1 software, respectively (both from Thermo Fisher Scientific).

In vitro cell growth assays

Designated cells lines were seeded in 96-well plates at density of 1,000 (TMZ-R) or 2,000 (TMZ-S) cells per well, with 4 replicates per treatment group. Cell viability was measured using CellTiter-Glo Luminescent Cell Viability Assay Kit (Promega) at designated timepoints according to the manufacturer's instructions. Luminescence was measured using SpectraMax M3 Multi-Mode Microplate Reader (Molecular Devices) and normalized to the luminescent readings at day zero or DMSO control.

Oxygen consumption rate and extracellular acidification rate

Oxygen consumption rate (OCR) was measured in an XF96 extracellular flux analyzer (Agilent Bioscience). Designated cells were plated at 10k cells per well of an XF96 plate and allowed to adhere for 48 h. At 1 hr before OCR measurement, the medium was exchanged for Seahorse base DMEM pH 7.4 (Agilent catalog no. 103575-100, supplemented with pyruvate, glucose, and glutamine). Electron transport chain inhibitors (1.5 μM Oligomycin, 0.5 μM FCCP, 0.5 μM Rotenone/Antimycin A) were injected according to the Seahorse XF Cell Mito Stress Test template (Agilent catalog no. 103015-100). After assay completion, XF Seahorse Mito Stress Test data was exported and analyzed in excel and Prism with the provided macros.

MitoTracker mitochondrial mass and imaging assay

Cells were seeded at 2,500 cells/well in a white-walled optical density 96-well plate. After overnight attachment, cells were stained with MitoTracker Green FM (Thermo M7514) per manufacturer's instructions. Fluorescence was read using the SpectraMax M3

Multi-Mode Microplate Reader (Molecular Devices). For localization assays, 35,000 cells were seeded in a 12-well plate and allowed to attach overnight. The next day cells were stained with MitoTracker Green FM (Thermo M7514) per manufacturer's instructions and treated with either DMSO or nocodazole (10 nM) for 45 min and imaged on a Nikon Eclipse Ti-U.

Immunofluorescence assays

Cells were seeded at a density of 25,000 to 30,000 cells onto 18-mm-diameter #1.5 round coverslips (VWR, #101413-518) in 12-well dishes (day 1). They were allowed to attach to the coverslips for a full day (day 2). In the case of treatments, N-acetylcysteine, GTP, GSHee, Glycine, are performed on Day 2 for 18 h to still be imaged on day 3. On the following day (day 3), the media was removed, and cells were washed three times with phosphate-buffered saline (PBS) and then fixed and permeabilized in 3.2% paraformaldehyde (PFA) with 0.2% Triton X-100 in PBS for 5 min at room temperature. Three washes were performed with PBS in the 12-well plate, and then coverslips were inverted onto 120 μL of primary antibody in the antibody block (0.1% gelatin with 10% normal donkey serum in distilled H_2O) on strips of parafilm and incubated for 2 h. Coverslips were first incubated with EWSR1 (rabbit monoclonal antibody; 1:600; Abcam, ab133288; mouse monoclonal antibody; 1:200; SCBT, sc-48404), for 4 h. The donkey serum, nonconfluent cells, 4-h incubation for primary antibodies, and day 3 staining are vital for visualizing consistent EWSR1 cytoplasmic staining. After incubation with primary antibodies, coverslips were washed three times with PBS. Then, coverslips were inverted onto 100 μL of antibody block with secondary antibodies (Alexa Fluor 488 anti-mouse; 1:200; Life Technologies, #A11029; Alexa Fluor 594 anti-rabbit; 1:200; Life Technologies, #A11037) and 4′,6-diamidino-2-phenylindole (DAPI) (DNA, 1:500 dilution) for 20 min in the dark. Coverslips were again washed three times with PBS, then gently dipped four times into molecular biology-grade water before inversion onto one drop of Fluoro-Gel (with N-tris(hydroxymethyl)methyl-2-aminoethanesulfonic acid buffer, Electron Microscopy Sciences, #17985-30), and then allowed to air dry in the dark for at least 10 min. Slides were stored at 4°C until image collection on an Olympus BX-53.

Immunoblot and immunoprecipitation analysis

Cells were lysed in radioimmunoprecipitation assay buffer supplemented with protease and phosphatase inhibitors (Roche, #4906837001) for protein extractions and separated by polyacrylamide gel electrophoresis using 4 to 12% gradient gels (Novex by Life Tech, #NP0321BOX) as described previously. Proteins were then transferred onto Nitrocellulose membranes (Invitrogen, #IB23001) with the iBlot2 (Invitrogen, #IB21001) and probed with the following antibodies: EWSR1 (1:1000; Abcam, ab133288), pyroglutamic acid (LSBio LS-C664190) and GGCT (Proteintech 16257-1-AP). Proteins were detected with horseradish peroxidase (HRP)–conjugated secondary antibodies (Promega Anti-Mouse HRP conjugate, W4028; Anti-Rabbit HRP conjugate, W4018). Blots were developed with enhanced chemiluminescence (Cytiva RPN2106V1, RPN2106V2) reaction according to the manufacturer's instructions and imaged on an Invitrogen iBright 1500 (ThermoFisher).

ROS detection

Cells were seeded in a clear bottomed white-walled 96-well microplate (Costar, 3610) at 5,000 cells/well and allowed to adhere for 48 h. Media was removed and replaced with 100 μL 1X buffer. This was replaced with the DCFDA diluted solution as per manufacture's protocol and incubated for 45 min at 37°C in the dark. DCFDA solution was then removed and washed with PBS and read on a SpectraMax M3 Multi-Mode Microplate Reader (Molecular Devices) at 485/535 Ex/Em.

Gene expression analysis in glioma single cell (sc)RNA-seq dataset

A published scRNA-seq data[63] in seven IDH-WT and seven IDH-mut gliomas was used to analyze GGCT and complex III expression in different glioma cell states and types. The gene expression matrix was downloaded from NCBI's Gene Expression Omnibus (GEO) database with dataset ID GSE151506. The clinical information of each sample as well as the cellular state assignment were obtained from the supplementary data of previous publication.[63]

Immunohistochemistry (IHC) analysis

Matched pairs of new and recurrent glioblastoma patient tissue samples, as well as Alzheimer's brains and cognitively normal brains were stained using standard IHC analysis using the following antibodies: EWSR1 (Abcam ab133288) diluted at 1:1000, pyroglutamic acid (LSBio LS-C664190) diluted at 1:200 and GGCT (Proteintech 16257-1-AP) diluted at 1:500. Four-micrometer thick sections of formalin-fixed paraffin-embedded (FFPE) tissue on charged slides were baked in the oven before being deparaffinized and re-hydrated. Antigen retrieval was performed using a pH6 retrieval buffer (Biocare Reveal) at 110°C for 10 min in a decloaking chamber. Slides were then cooled to room temperature and washed in TBS before neutralizing endogenous peroxidase (Biocare Peroxidase 1). Slides were then treated with a serum-free casein background block (Biocare Background Sniper) before preincubation in a 10% goat serum block for 60 min. Primary antibody was then added to the slides for overnight incubation at 4°C. After incubation, slides were washed well with TBS-T before incubating in HRP polymer (Biocare MACH 4 Universal HRP Polymer). Finally, reaction products were visualized with DAB (Biocare Betazoid DAB Chromogen Kit). Slides were then counterstained with hematoxylin, dehydrated and mounted with xylene-based mounting media. Slides were stored at 4°C until image collection at 60X on an Olympus BX-53.

QUANTIFICATION AND STATISTICAL ANALYSIS

Statistical analysis

Statistical analyses were carried out using GraphPad Prism version 10. All grouped data are from distinct biological replicates. For comparing two groups, the two-tailed Student's t-tests were used unless otherwise stated. Graphs include means and error bars, with the latter representing SD as indicated. Statistical significance was calculated by one-way analysis of variance (ANOVA) with Tukey's multiple comparisons test or unpaired *t* test. All error bars are SD; $^{*}p < 0.05$, $^{**}p < 0.001$, $^{***}p < 0.0005$, and $^{****}p < 0.0001$. All analyses were done with at least 3 independent replicates.

Data availability

All data produced is included in a supplementary table or a citation from which the scRNAseq data was acquired (See scRNAseq methods).